Femtosecond Resonance-Enhanced Multiphoton Ionization of Perylene in Hexane. Electronic Excitation of the Radical Cation and Evidence of Hydrogen Abstraction from the Solvent

Jesse S. Greever, Joseph B. M. Turner, and John F. Kauffman*

Department of Chemistry, University of Missouri, Columbia, Missouri 65211

Received: December 31, 2001; In Final Form: January 14, 2003

We demonstrate that perylene in solution can be highly excited with relatively weak femtosecond radiation via two-photon resonance-enhanced multiphoton ionization and excitation. The femtosecond multiphoton excitation spectra of two different observables are presented for perylene dissolved in hexane. The first of these is the normal $S_1 \rightarrow S_0$ fluorescence that arises from relaxation of perylene through the singlet manifold after multiphoton excitation. The second observable is the ion yield that results from multiphoton ionization. A comparison of these two excitation spectra is presented, and their striking similarity indicates that both processes occur via the same initial two-photon resonance in the 500−550 nm region. A mechanism is presented illustrating the predicted excitation and relaxation pathways. The multiphoton-excited emission spectrum of the sample exhibits anomalous emission in the 550−620 nm range. Comparison of this emission with the one-photon-excited emission spectrum of perylene in concentrated sulfuric acid shows that the anomalous emission originates from electronic excitation of cationic species present in sulfuric acid. Previous assignment of emission from perylene dissolved in sulfuric acid to the protonated cation implies that the perylene radical cation in hexane abstracts a hydrogen atom from the solvent on an ultrafast time scale.

Introduction

In recent years, several groups have demonstrated that complex photochemistry following high-power laser irradiation of condensed phase samples can yield to careful experimental examination, resulting in applications for chemical analysis and a deeper understanding of the rich chemistry of highly excited molecules in condensed phases. For example, Webb and co-workers have demonstrated that the four-photon excitation of 5-hydroxyindoles results in chemical species that fluoresce under two-photon excitation,[1] and Shear and co-workers have shown that dissolved oxygen reduces the formation efficiency of the fluorescent photoproduct.[2] These discoveries have resulted in the development of extremely sensitive methods for analysis of neurotransmitters and their metabolites. Ogawa and co-workers have studied multiphoton ionization of polycyclic aromatic hydrocarbons (PAHs) extensively using nanosecond lasers.[3−8] They have shown that multiphoton ionization of polycyclic aromatic hydrocarbons can proceed through a simultaneous multiphoton absorption process, or through a stepwise process, in which the photoion is produced via photon absorption by an excited molecule following population of the S_1 state via two-photon excitation.[9] In the latter case, the use of nanosecond lasers is essential, because vibrational relaxation typically occurs on a time scale of tens of picoseconds or longer. Brede et al.[10] have performed a direct comparison of femtosecond versus nanosecond multiphoton excitation of sterically hindered substituted phenol in liquid solution. They have shown that the photoproduct of the femtosecond excitation process is a phenol radical cation, whereas nanosecond excitation yielded a phenoxy radical. They interpreted the former process as direct multiphoton ionization of the solute. Under nanosecond excitation the authors argue that the initial excitation populates the highly acidic S_1 state of the substituted phenol, which then isomerizes to a configuration that undergoes simultaneous photoinitiated ionization and deprotonation, resulting in the phenoxy radical product.

The two latter examples illustrate one of the essential differences between femtosecond and nanosecond multiphoton-excited photochemistry. Because many relaxation phenomena occur on the picosecond-to-nanosecond time scale, multiple reaction pathways are likely to occur following nanosecond laser excitation, whereas femtosecond excitation is fast on the time scale of most relaxation phenomena. Energy thermalization resulting from these phenomena will result in sample heating on a nanosecond time scale, which is an additional complicating phenomenon that can be avoided with femtosecond excitation, at least within the duration of the laser pulse. Long-time sample heating will, of course, occur under all excitation conditions, but this effect is much more severe for a single 10-ns pulse than for a train of 1000 pulses of 100 fs duration and similar peak power, the latter being typical of experiments performed with amplified Ti:sapphire lasers. On the other hand, in situations where narrow bandwidths are required, nanosecond lasers may still be preferable to femtosecond lasers.

Recent advances in the photochemistry of highly excited PAHs have benefited from the convergence of radiation chemistry and ultrafast laser spectroscopy. In 1993, Trifunac and co-workers[11] observed a decrease in PAH radical cation population with increasing excitation energy following excitation with nanosecond UV irradiation. On the basis of photoproduct analysis, they postulated that excited PAH radical cations undergo deprotonation followed by hydrogen abstraction to create both solvent radicals and protonated cations, thereby

* Author to whom correspondence should be addressed. E-mail: kauffmanj@missouri.edu.

10.1021/jp014670i CCC: $25.00
Published on Web 04/24/2003

depleting the radical cation population. Later, Shkrob, Trifunac, and co-workers measured the dc photoconductivity of cyclohexane solutions of PAHs following nanosecond UV laser photoionization, and proposed that the electronically excited solute relaxes via "hole injection" into the solvent.[12,13] In this mechanism, a solvent molecule transfers an electron to the electronically excited PAH radical cation. Through the use of delayed excitation of the precursor radical cation, they demonstrated that, while the ground-state PAH radical cation is relatively stable, the excited-radical cation is highly reactive. On the basis of these and other studies, they were able to identify solvent cations as the "high-mobility ion" that had been previously observed in pulse radiolysis of these solvents.[14,15] Subsequent studies in polar solvents suggested the possibility of hydrogen abstraction from the solvent by electronically excited PAH radical cations when the excited PAH radical cation is more basic than the solvent.[16] Around this time, Vauthey and co-workers[17,18] had undertaken an investigation of the dynamics of electronically excited radical cations, including perylene, using picosecond transient grating spectroscopy. They prepared PAH radical cations by irradiation of various glasses doped with PAHs, dissolution of PAHs in concentrated sulfuric acid, and photoinduced electron transfer to acceptors in acetonitrile. In the solution phase they measured excited-state lifetimes of less than 15 picoseconds, while the lifetime in the solid was 35 picoseconds at room temperature, and increased with decreasing temperature. Their data suggested that relaxation of the electronically excited PAH radical cations proceeded through intermolecular quenching, possibly including a reversible charge transfer reaction with the solvent. These results also indicate that the electronically excited radical cations are highly reactive, whereas the radical cations are relatively stable. Kohler and co-workers[19] have surmised that indole radical cations react with solvated electrons in water at a rate that is significantly slower than the diffusion limit, which also highlights the stability of the ground-state radical cation.

We have recently observed anomalous emission from a solution of perylene in hexane irradiated with femtosecond radiation in the 540−460 nm range. The purpose of this paper is to present a photochemical mechanism that explains this phenomenon. The mechanism proposes preparation of an electronically excited perylene radical cation ($Pe^{\bullet+*}$) via resonantly enhanced multiphoton ionization, followed by a fast photochemical reaction. Yu et al. explored the two-photon excitation spectrum of perylene in *n*-hexane in the 560−770 nm region, which showed a number of excitation maxima above 573 nm.[20] They compared the observed transitions with theoretically predicted energies and previous literature values for electronically excited states of perylene. On the basis of two-photon excitation selection rules, tentative symmetries were assigned to the excited states. In this paper, we extend the multiphoton excitation spectrum of perylene in hexane, covering the range from 460 to 600 nm. We present evidence for a two-photon resonance enhancement of the one-photon emission spectrum and a concomitant enhancement in the multiphoton ionization yield. Anomalous emission in the 550−620 nm range becomes apparent in the resonance enhancement region of the excitation spectrum, giving rise to emission that appears white to the unaided eye. We propose that these three observables are branches of the same "parent" two-photon excitation process in the wavelength region under study. The spectrum of the anomalous emission is similar to emission observed from perylene dissolved in concentrated sulfuric acid, which has been previously assigned to emission from the protonated perylene cation. (See ref 18 and references therein.) This photoproduct suggests that the electronically excited perylene radical cation abstracts hydrogen from the hexane solvent.

Experimental Section

Perylene was obtained from Aldrich at 99%+ purity and used as received. Hexanes (Optima Grade) and sulfuric acid were obtained from Fisher and used as received. All solutions were 5×10^{-5} M in perylene. The experimental setup for measuring femtosecond multiphoton-excited conductance spectra (fs-MPECS) has been described previously.[21] Briefly, a tunable optical parametric amplifier (1-kHz rep rate, ∼1 mW average power, ∼150 fs pulse width) is tuned incrementally over the range of 460−620 nm, while being kept at a constant photon density. This is achieved by monitoring the intensity with a photodiode, correcting for wavelength, and carefully adjusting a circular variable neutral density filter. Saturation effects are observable near the upper limit of the OPA's output power range, and these effects have been thoroughly examined in our previous paper.[21] Therefore, the operating photon density is chosen to avoid saturation across the range of wavelengths of interest. The pulses are focused between two stainless steel electrodes separated by 0.8 mm inside a standard 1-cm quartz fluorescence cell that contains a 5×10^{-5} M solution of perylene in hexane. The laser spot size is approximately 100 μm in the center of the electrodes, which is also the spectrometer viewing region. A high voltage (∼1000 V) is applied and the ion yield due to multiphoton ionization is measured by monitoring the current across the electrodes. The current signal from the electrodes is converted to a voltage and amplified using an *I*/*V* converter (calibrated gain of 2.02×10^8 volts/amp). The amplified signal is sampled and held and delivered to an analog-to-digital converter (Data Translation DT2812). The final signal resulted from averaging 10 000 laser shots per data point. The ionization signal is plotted versus excitation wavelength, and a photoionization excitation spectrum is obtained. The solvent photoionization excitation spectrum was collected prior to perylene solution measurement, and contributed approximately 5% to the overall photocurrent at each wavelength.

Sample fluorescence was collected through a microscope objective using the same excitation source and sample cell, with a computer-controlled motorized monochromator (ISA H-10, reciprocal linear dispersion = 8 nm/mm, 1.0 mm slits) and a R928 Hamamatsu PMT situated perpendicular to the excitation beam. The PMT signal is sampled and held and delivered to an analog-to-digital converter (Data Translation DT 2812). The signal was integrated over 1000 excitation pulses and recorded for each excitation wavelength to obtain a multiphoton-excited fluorescence excitation spectrum. An excitation wavelength of 535 nm was used to measure the multiphoton-excited emission spectrum, and the emission monochromator was scanned across the spectral region of interest.

Multiphoton-Excited Fluorescence and Conductance Excitation Spectra. The rate of formation of excited species generated by a general *n*-photon excitation process is given in eq 1.[22]

$$\frac{\mathrm{d[M^*]}}{\mathrm{d}t} = \delta_n(\lambda)\{I(\lambda)\}^n[\mathrm{M}] \qquad (1)$$

The formation rate of the excited species, M*, is dependent upon the initial concentration of the molecule, [M], the wavelength-dependent *n*-photon excitation cross section, $\delta_n(\lambda)$, and the wavelength-dependent excitation intensity factor, $I(\lambda)$, given as

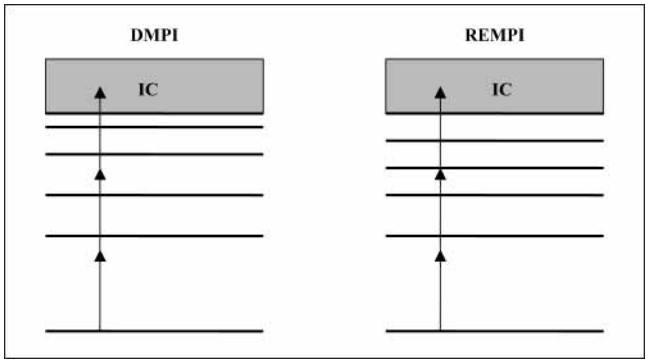

Figure 1. Representative energy level diagrams for direct nonresonant multiphoton ionization (DMPI) and (2+1)-resonance-enhanced multiphoton ionization (REMPI). The left diagram shows direct excitation into the ionization continuum (IC). The right diagram shows a two-photon resonance with a high-lying excited state in the process of three-photon ionization. The two-photon resonance enhances the number of molecules ionized by increasing the overall multiphoton ionization cross-section.

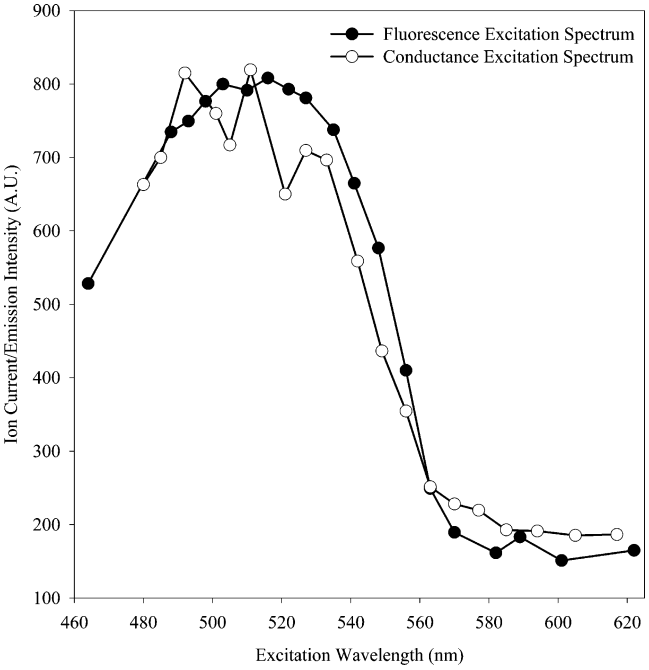

Figure 2. Fluorescence and photocurrent excitation spectra. The vertical scale is arbitrary, and the ion current is normalized to the fluorescence intensity scale.

photon flux (photons cm^{-2} s^{-1}). When the overall energy of excitation exceeds the ionization potential of the molecule, multiphoton ionization (MPI) can occur. The rate of formation of cations, M^+, is a special case of eq 1, where the cross-section factor is the MPI cross-section. Both direct multiphoton ionization (DMPI) and resonance-enhanced MPI (REMPI) can occur, as illustrated in Figure 1.

The multiphoton-excited fluorescence excitation spectrum of perylene is presented in Figure 2, along with the multiphoton-excited conductance excitation spectrum. The fluorescence excitation spectrum is collected at an emission wavelength of 450 nm, and represents the $S_1 \rightarrow S_0$ emission arising from molecules that relax to the S_1 state following two-photon excitation to a highly excited S_n state. A large enhancement of the signal in the 500−540 nm region gives reason to believe that a two-photon resonance occurs in that range. Figure 3a is a plot of the excitation power dependence of the 450 nm perylene emission following excitation at 535 nm. The solid

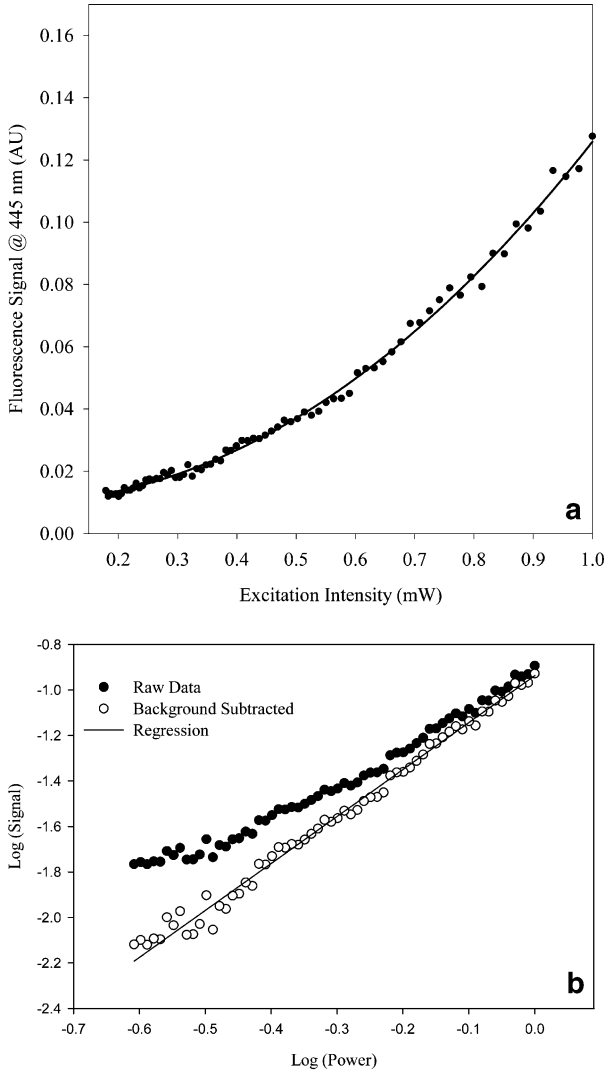

Figure 3. (a) Excitation intensity dependence of 450 nm emission of 5×10^{-5} M perylene in hexane excited at 535 nm. The fitted power law exponent is 2.08, which is consistent with a two-photon dependence. (b) A log−log plot of the excitation intensity dependence of the emission. Curve-fitting results appear in Table 2.

line is a fit to an intensity power law having the form $S = \alpha P^{\gamma} + S_0$, where P is the incident laser power, S_0 is the background signal level, α is a fitting parameter associated with the cross section of the nonlinear process of interest, and the exponent γ is the photon order of the nonlinear process. The exponent has a value of 2.08, and is consistent with a two-photon resonance enhancement. This evidence suggests that a two-photon resonant state exists in the 250−270 nm range. Analysis of Figure 3 is discussed in more detail below.

Perylene has a highly congested electronic and vibrational manifold, and as a result, a number of two-photon resonances can potentially occur over our wavelength range of study. Yu et al. presented a number of possible assignments of high-lying excited vibronic states for perylene in *n*-hexane.[20] Matsunuma et al. calculated the positions of possible two-photon resonant states in their study of $S_1 \rightarrow S_n$ transitions of perylene using a configuration interaction (CI) method.[23] Meyer and Plaza[24] measured a strong $S_1 \rightarrow S_n$ transition at 700 nm, which suggests the existence of a symmetry-forbidden electronic state with its origin at 268 nm. Birks also provides a list of some of the excited states of perylene in heptane.[25] A compilation of these values appears in Table 1. Both Birks and Matsunuma place an excited state between 37000 and 38000 cm^{-1}, and Matsunuma

TABLE 1: Energy Level Assignments by Three Different Sources[a,b,c]

excited states[a] (cm^{-1})	two-photon wavelength (nm)	excited states[b] (cm^{-1})	two-photon wavelength (nm)	excited states[c] (cm^{-1})	two-photon wavelength (nm)
		25000 (B_{1u}^+) [S_1]		23000 [S_1]	
26530 ($B_{3u}^- + b_{2u}$)	754				
27860 ($B_{1g}^- + b_{2u} + a_g$)	718				
		30570 (B_{3g}^-)	654		
32000 (?) (B_{1g}^-)	625				
33780 ($A_g^- + b_{1g}$)	592				
34900 ($A_g^- + a_g$)	573			34300	583
		35670 (A_g^-)	561		
		37120 (B_{3g}^-)	539	38000	526
		44790 (A_g^-)	447	44000	455
		48510 (B_{3g}^-)	412	48500	412

[a] Ref 28. [b] Ref 29. [c] Ref 27.

assigns this state to a B_{3g}^- symmetry. This corresponds with a two-photon resonance between 526 and 540 nm, which supports our conclusions based on Figure 3. Although the information provided by Birks does not include a symmetry assignment, the small absorption coefficient reported for this state is consistent with one-photon forbidden symmetry.

Following the two-photon resonant excitation, we postulate that perylene may undergo one of two processes. The first process is relaxation to the S_1 excited state, followed by radiative relaxation to the ground state, giving rise to the emission spectrum that is expected under normal one-photon excitation. The second process is the absorption of an additional photon to ionize the molecule. The external electric field applied across the excitation zone allows us to capture a fraction of the electrons and cations generated by this process, giving rise to the photocurrent spectrum. The similarity of the emission and ionization excitation spectra provides evidence that the two pathways arise from the same initial process. At 540 nm, three-photon absorption terminates well into perylene's liquid phase ionization continuum, as discussed in more detail below. If the density of states is high in this region, the absorption cross-section from the high-lying excited state to the ionization continuum is expected to be relatively insensitive to excitation wavelength. Charge capture in the presence of an electric field is also expected to be insensitive to wavelength. Siebbeles et al. [26] have shown that for electron energies in excess of ~1 eV, electron thermalization lengths in alkanes are in the range of 25 to 70 Å, whereas the Onsager escape distance for an electron in alkanes is ~300 Å. In the absence of an electric field, the perylene radical cation and electron will eventually recombine. When the external field is applied, the electron experiences a field that equals that of the cation core when the electron is at a distance in excess of 200 Å. Thus, the external field will capture the outer tail of the thermalized electron distribution as well as electrons that migrate to the capture distance following thermalization. From the results presented here, we surmise that this process is also relatively insensitive to excitation wavelength, and as a result the MPECS spectrum is dominated by the influence of the two-photon resonant transition.

Analysis of Power-Dependent Emission and Conductance. The excitation intensity dependence of the photocurrent is shown in Figures 4a and 4b. We model the signals in Figures 3 and 4 using the expression $S = \alpha(\bar{P} + \delta_P)^\gamma + (\bar{S}_0 + \delta_{S_0})$, where $\bar{P}$ is the average power at a given attenuation, δ_P is an error term associated with random power fluctuations, $\bar{S}_0$ is the average background signal, and δ_{S_0} is an error term associated with random background fluctuations. The fitting parameters α and γ are related to the process cross-section and the photon order,

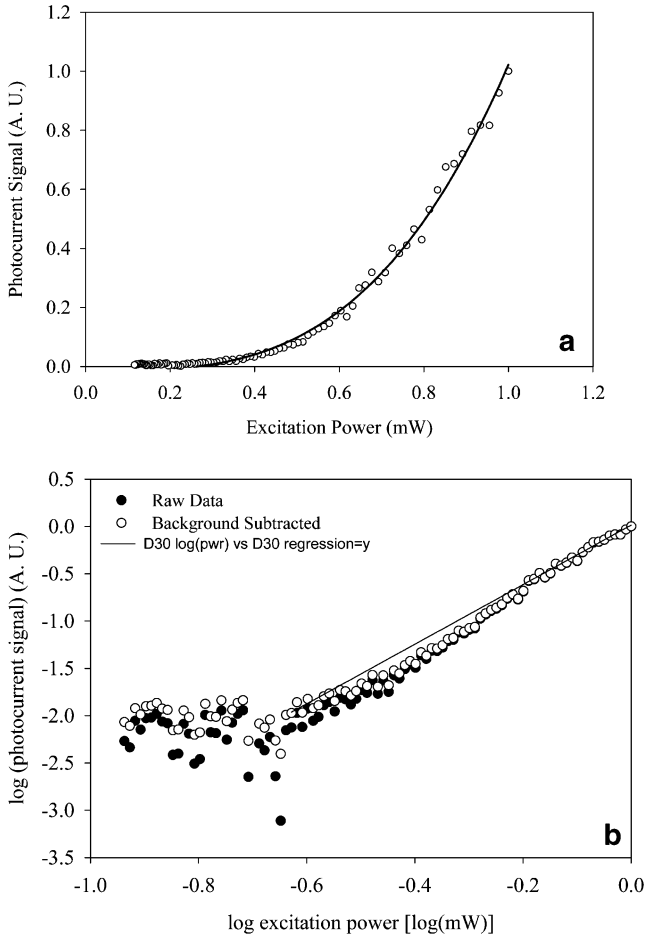

Figure 4. (a) Excitation intensity dependence of the photocurrent of 5×10^{-5} M perylene in hexane excited at 535 nm. The fitted power law exponent is 3.19, which is consistent with a three-photon dependence. (b) A log−log plot of the excitation intensity dependence of the photocurrent. Weighted linear regression analysis gives a slope of 3.15. Curvature in the plot is evident. Curve fitting results appear in Table 2.

respectively. This analysis is aimed at extracting the photon order of the processes that have been presented in Figures 3 and 4.

To begin, we dispense with the power fluctuation term by the following argument. $\bar{P}$ is related to the average maximum source intensity ($\bar{I}$) by the attenuation factor, $K = \bar{P}/\bar{I}$. Thus $\bar{P} + \delta_P = K(\bar{I} + \delta_I)$, $\delta_P = \bar{P}/\bar{I}\delta_I$, and therefore

$$S = A\bar{P}^\gamma + (\bar{S}_0 + \delta_{S_0}) \qquad (2)$$

TABLE 2: Fitting Parameters of Emission and Photocurrent Power Dependence Measurements[a]

	power law fit				linear regresion of log−log data		
	S_0	A	γ	R^2	A	γ	R^2
emission	0.00956	0.1163	2.08	0.996	−0.935	2.06	0.994
photocurrent							
full	−0.00316	1.0321	3.31	0.994	0.011	3.22	0.978
D20	−0.00974	1.034	3.24	0.994	0.0138	3.19	0.982
D30	−0.015	1.037	3.19	0.994	0.015	3.15	0.984

[a] S_0 from each power law fit is subtracted from the signal before the log−log transformation. The log−log data are analyzed using weighted linear regression, as discussed in the text. With proper weighting and background subtraction, truncation has a minimal effect on the fitting parameters.

where $A = \alpha(1 + \delta_I/\bar{I})^\gamma$. Monte Carlo simulation of this factor indicates that its standard deviation is equal to the standard deviation of the excitation intensity, magnified by a factor equal to the photon order of the process under study, thereby contributing to curve-fitting uncertainty. However, intensity fluctuations do not directly influence the value of the exponent that is extracted from analysis of the signals power dependence. (Monte Carlo simulation was performed in Microsoft Excel using the Crystal Ball add-in, Decisioneering, Inc.) Two methods have been used to extract γ from the data. First we have performed a nonlinear regression using a 3-parameter power law model function. The results are given in Table 2, and demonstrate that the emission is of order 2.08 in the laser power, and the photocurrent is of order 3.2 to 3.3, depending on how much of the low-power data is truncated. We discuss truncation below.

The second method to extract photon order is linear regression analysis of the log−log plot of the data, shown in Figures 3b and 4b. The log−log plots amplify the low-signal portion of the graphs. In Figure 3b, the influence of background signal on the linearity of the log−log plot is apparent, while Figure 4b demonstrates the influence of detector noise on the low-signal limit of the measurement. Both of these factors must be considered when extracting exponents from log−log plots. From eq 2, it is apparent that background must be subtracted from the signal before making the log−log transformation. The nonlinear regression analysis offers an objective means of assigning background levels, and in the analysis that follows we have used the power-independent term from the power law fit of each data set as the subtracted background for each log−log plot linear regression analysis presented. Figures 3b and 4b show the data before and after background subtraction.

To properly fit the log−log data to the linear model function, weighting factors that reflect the dependence of the variance of the data on signal level must be used. Assuming that (1) the correct weighting factor is the inverse variance of each data point, and (2) the signal variance is primarily due to detector noise, which is independent of signal level, nonlinear regression analysis can be carried out with equal weights. However the variance of $\log(S - S_0)$ scales as $(S - S_0)^{-2}$, since $\sigma_{\log(S-S_0)}^2 = [\mathrm{d}(\log(S - S_0))/\mathrm{d}S]^2\sigma_S^2$. Thus the correct results can only be anticipated when the linear regression of the log−log plot is weighted by $(S - S_0)^2$. The weighted linear regression of the log−log emission data gives an exponent of 2.06, which is consistent with the power law analysis.

Finally, the amplifier used to collect the photocurrent signal has a relatively high noise floor in comparison with fluorescence. The latter effect can be seen in Figure 4b, where the low-power data reflect background noise, and the issue of truncation of the low-signal photocurrent data must be addressed. We have tabulated the results of our linear regression analysis of the log−log data in Table 2 for the full data set, the same data set with the lowest 20 data points truncated (D20), and the same data set with the lowest 30 data points truncated (D30). The results indicate that the photocurrent exponent is 3.2. We also note that an unweighted linear regression analysis of the D30 data set gives an exponent of 3.53, a significant deviation from the result of the power law regression analysis. The line in Figure 4b shows the prediction based on the linear regression parameters extracted from the D30 data set. This nonintegral value is close to 3, and therefore is consistent with a three-photon ionization process.

The regression line in Figure 4b highlights the curvature of the data. Several factors may explain the super-tertiary photon order of the photocurrent data. Multiphoton-excited photocurrent data also contain solvent background that complicates data analysis. Unlike fluorescence data, we can anticipate signal contribution from the solvent, as illustrated by our previous study of photoionization of neat solvents.[21] Though this is a small contribution to the total photocurrent signal, it cannot be easily subtracted from the solution signal, because the nonlinear absorption due to perylene and associated thermal effects will influence the beam conditions in the photocurrent collection zone. In addition, we will demonstrate in a later section that the ions we create are also electronically excited, and on the basis of the calculated liquid-phase double ionization potential of perylene,[27] we suspect that multiple ionization may also be possible via a six- or seven-photon process. Thus the conductance data is a combination of a three-photon-excited single ionization, a higher-order double ionization, and solvent ionization, and this will affect the observed power dependence. At high intensity, the signal is strong enough that thermal effects and light scattering in the front half of the cuvette may also result in saturation of the signal. We suspect that solvent ionization, which is a 4th-order process for hexane at this wavelength,[21] and the possible contribution from a 6th- or 7th-order double ionization pathway contribute to the observed super-tertiary photon order as well as curvature in the log−log plot. Preliminary kinetic analysis of the excitation scheme shown in Figure 5 suggests that nonintegral, power-dependent photon order may arise when multiple excitation pathways are accessible. Further kinetic analysis of this scheme is in progress. With these caveats and in light of the analysis presented below on the ionization potential of perylene in solution, we are confident that three-photon ionization is primarily responsible for the perylene contribution to the photocurrent presented in Figure 4.

Ionization Potential of Perylene in Solution. The liquid-phase ionization potential of perylene can be calculated from the gas-phase ionization potential ($\mathrm{IP_g}$), the ion solvation energy (P_{pol}), and the conduction band energy of the liquid (V_0), shown in eq 3.

$$\mathrm{IP_l} = \mathrm{IP_g} + P_{pol} + V_0 \tag{3}$$

P_{pol}, also referred to as the solvent polarization term, is derived from the Born Continuum Solvation Model (BCSM),[28] which describes the solvation energy of a point charge in a spherical cavity immersed in a dielectric continuum, and is given by

$$P_{\mathrm{pol}} = -\frac{1}{8\pi\epsilon_0}\left(1 - \frac{1}{\epsilon}\right)\left(\frac{q^2}{r}\right) \tag{4}$$

where ϵ is the dielectric constant, r is the van der Waals radius of the solute, and q is the charge of the cation. V_0 corrects for

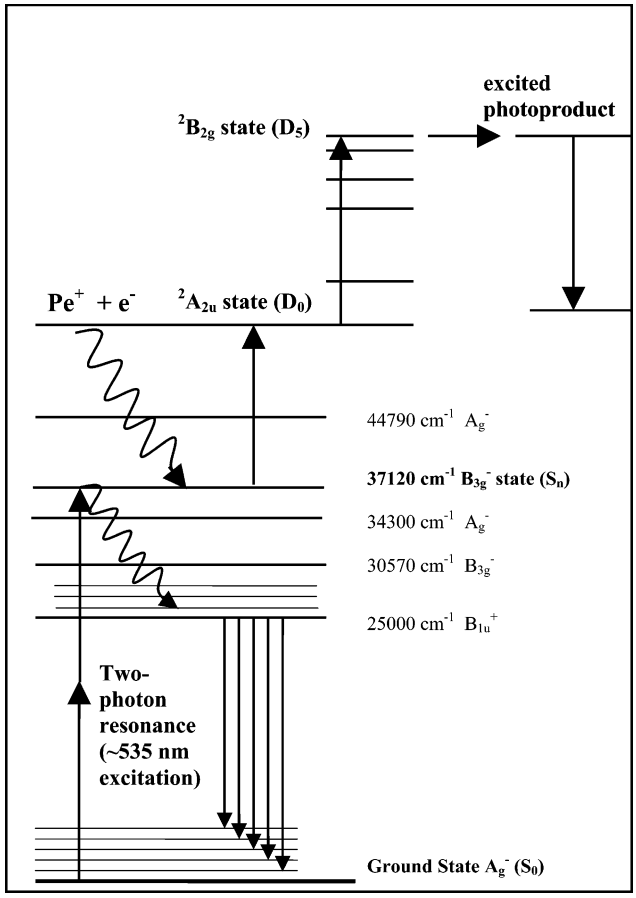

Figure 5. Perylene energy level diagram. The diagram presents the proposed pathway for simultaneous generation and excitation of the perylene radical cation. The first step is a two-photon resonance with a high-lying singlet state (S_n), followed by the absorption of an additional photon to promote the perylene to the ionization continuum. The perylene radical cation absorbs another photon and is promoted to the D_5 state, where it can emit back to the ground cationic state (D_0).

the electron solvation energy, and is usually the least significant term in eq 3. For DMPI of neat nonpolar liquids, we demonstrated excellent agreement between the measured ionization potential of pure liquids using MPECS and theoretical values from eqs 3 and 4 using Bondi's method for determining the van der Waals radius.[29] Katoh[30] has also shown that van der Waals radii are appropriate measures of ionic radii when applying the BCSM to polycyclic aromatic hydrocarbon cations. The Bondi method yields a van der Waals radius of 3.77 Å for perylene. Using the gas-phase ionization potential of perylene (6.96 eV), the ionization potential of perylene in hexane is found to be 6.06 eV (~205 nm). Furthermore, Tobita et al.[27] have found the double ionization potential of perylene to be 18 eV in the gas phase, and application of the above model indicates that a liquid-phase ionization potential in the range of 14.6 eV (84.9 nm) is anticipated. Six photons at 535 nm delivers 14 eV of energy to perylene. Thus double ionization via femtosecond multiphoton excitation is possible with the absorption of 3 or 4 additional photons following three-photon ionization. The following discussion indicates that the above value of 6.06 eV is a reasonable value for the ionization potential of perylene in hexane. We then discuss the likelihood of double ionization.

The theoretically predicted liquid-phase ionization potential of perylene contradicts the ionization potential determined by Christophorou et al.[31] In these studies, determinations of the ionization potentials of the solute molecules are ascertained by one of two strategies. The first strategy exploits the nonlinear intensity dependence of the ion yield governed by eq 1.[32,33] The authors assume that near the transition in which n photons are no longer sufficient to ionize, the form of the intensity dependence of the photocurrent is a linear combination of n- and $(n + 1)$-photon ionization events. They determine the $(n + 1)$-photon ionization onset to be the wavelength when the best fit for the intensity dependence is $I^{(n+0.9)}$. According to the authors, this is the point where the ionization process is 10% n-photon and 90% $(n + 1)$-photon. The second strategy employed by Christophorou et al. is to compare excitation spectra of the integrated emission in the presence and absence of extremely high concentration (>1 M) electron attaching species to the normal one-photon absorption spectrum and assigning the most striking incongruence to the onset of ionization.[31,34] However, this study was performed in a 1:7 mixture of n-hexane in perflourohexane, and therefore is actually a determination of the ionization onset of perylene in a binary mixed solvent. Using this method, the authors determine the ionization potential of perylene in hexane to be approximately 5.3 eV, approximately 0.7 eV less than the BCSM prediction.

Other studies by Holroyd and Ogawa tend to agree with the BCSM prediction.[6,35,36] Holroyd et al. performed single-photon conductivity measurements and present experimentally determined solution-phase ionization potentials of perylene in 2,2,4-trimethylpentane (TMP) and tetramethylsilane (TMS).[35] On the basis of the dielectric constants and conduction band energies of TMP, the predicted BCSM solution-phase ionization energies are 5.79 and 5.50 eV, respectively. This compares very well with the experimentally determined values of 5.78 and 5.47 eV, and supports the adequacy of 3.77 Å as a cavity radius for perylene. Ogawa et al. report both single-photon and two-photon ionization studies of perylene in water at the surface of an electrode.[6,36] The BCSM prediction of the solution-phase ionization potential is 5.07 eV, which is in sharp contrast to their measured value of 5.9 ± 0.1 eV. They attribute this disparity to the nature of the environment at the surface of the electrode. But this may also result from a failure of the BCSM model for polar solvents, in which the major contribution to the dielectric constant is the orientational polarization. Solvent reorientation is slow compared with the time scale of the ionization event, and therefore the orientational solvent response plays a limited role in stabilizing the cation during ionization. If the refractive index of water is used to calculate the polarization energy, an ionization potential of 6.13 eV is predicted, which, given the simplicity of the approximation, is close to the experimental value of 5.9 eV. Partial orientational polarization or electron solvation may be responsible for the difference between these values.

Figure 5 provides an energy level diagram of perylene and a summary of the proposed pathways for the observed ionization. The energy level assignments are based on those by Birks[25] and Matsunuma.[23] The diagram shows an initial two-photon excitation to an upper electronic state identified by both Birks and Matsunuma, with a symmetry assignment of B_{3g}^- from the calculations by Matsunuma. After the two-photon excitation, perylene can relax into the S_1 state where it can then emit light, and relax into the vibrational manifold of the ground state. Excitation from the S_1 state to the ionization continuum is assumed to be negligible, because the relaxation step from the S_n to the S_1 state is expected to occur on the picosecond time scale,[37] which is significantly longer than the pulse width of the excitation (~150 fs). This is not the case when high-photon-flux nanosecond excitation sources are used. Additionally, the highly excited perylene can absorb an additional photon, which

is sufficient to ionize it. Following ionization, either the electron escapes the Coulombic forces of the cation or it recombines with a positive perylene. Recombination results in a highly excited neutral perylene (in a high-lying S_n state), which ultimately relaxes to the S_1 state and contributes to the $S_1 \rightarrow S_0$ fluorescence. The branching ratios of these processes are still under investigation.

Photon Order Transitions of Perylene Solution Photoconductivity. In our previous study of DMPI of neat nonpolar liquids,[21] we examined the MPECS photocurrent excitation spectrum of solvent ionization in order to determine the *n*- to $(n + 1)$-photon transition. We found that when the photon energy is increased across an energy range where the number of photons required to exceed the ionization threshold decreases from $n + 1$ to n photons, a sharp increase in the photoconductivity is observed. We argued that this effect results from an increase in the multiphoton ionization probability as the photon order decreases, and therefore the transition can be used to measure the ionization potential of neat liquids. Comparison of the experimentally determined transition energy with the liquid-phase ionization potential predicted by the BCSM gave excellent agreement, supporting the assignment of the observed transitions. For completeness, we briefly consider the possible assignment of the observed increase in photoconductivity to a photon order transition in perylene.

The discussion of perylene ionization potential in hexane solution indicates that its ionization potential is in the range of 6.05 eV. Thus, at wavelengths longer than 615 nm, four photons are required to ionize perylene, whereas only three photons are required below 615 nm, and we expect a photon order transition in the range of 615 nm. We examined this region of the perylene MPECS spectrum thoroughly, but despite our best efforts, we were unable to observe a photon order transition. In our previous study of neat liquids, these transitions were extremely weak, with a signal-to-noise ratio in the 3-to-5 range. In the case of perylene, we anticipate an even weaker signal, because its concentration is 5 orders of magnitude smaller than the solvent concentration. The MPECS feature in Figure 2 is large, having a magnitude that exceeds the neat solvent photocurrent by a factor of approximately 100. In addition, the transitions observed in the pure liquid measurements were very sharp, and occurred over a range of about 10 nm.[21] In contrast, Figure 2 exhibits a broad signal level transition, which occurs over a range of approximately 40 nm. Finally, in order for the signal level transition observed in Figure 2 to arise from a photon order transition, and also be consistent with the BCSM model, an unreasonably large cavity radius is required. However, Katoh[30] has shown that the van der Waals radius is an appropriate measure of the cavity size when applying the BCSM to polycyclic aromatic cations, which rules out photon order transition as a contributor to the photoconductivity feature observed in Figure 2. This discussion, along with the similarity of the emission and MPECS spectra shown in Figure 2, is consistent with the hypothesis that resonance enhancement is responsible for this feature in the multiphoton-excited photoconductivity spectrum of perylene in hexane.

Anomalous Emission from Multiphoton-Excited Perylene. Figure 6 presents the emission spectrum of perylene in hexane following excitation with femtosecond 535 nm radiation. We observe a broad, structured emission in the 550−700 nm range that exhibits peaks at 573 nm and 600 nm. The anomalous emission is roughly half as intense as the strong two-photon-excited one-photon emission from the sample. Allamandola et al. assigned the absorption spectrum of the matrix-isolated perylene radical cation.[38] The spectrum shows a number of sharp bands, the strongest of which occurs at approximately 535 nm, corresponding to the D_0 (^2A_u) $\rightarrow$ D_5 ($^2B_{3g}$) transition. The solution-phase REMPI results presented above indicate that a significant population of perylene radical cations is generated with 535 nm radiation as a result of the two-photon resonance enhancement. Figure 5 presents an energy level diagram that illustrates the proposed excitation pathway for generation and excitation of the perylene radical cation. The perylene ions are generated through a three-photon ionization mechanism that is enhanced when the excitation wavelength is in the 500−550 nm region, as discussed above. The resulting ions can absorb an additional photon and be promoted to the D_5 state. We postulate that the emission arises from photoproducts of reactions that occur between the excited radical cation and the solvent, as discussed below. The coincidence of the two-photon resonance in the neutral species manifold at 535 nm and the subsequent one-photon resonance in the ion's doublet manifold give rise to the potential for the simultaneous generation−excitation scenario.

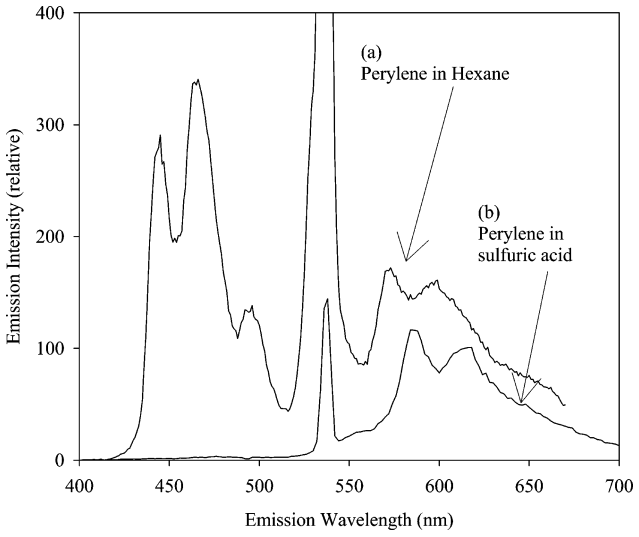

Figure 6. Overlaid emission spectra of (a) multiphoton-excited perylene in hexanes and (b) one-photon-excited perylene in sulfuric acid. The laser line for perylene in hexane is intense due to local heating effects as a result of ion−electron recombination and vibrational relaxation, which enhances scattering. Scattering is not as strong in the sulfuric acid solution, because the chemically generated ions present in solution absorb a single photon. Solutions are 5×10^{-5} M perylene.

To verify the nature of the emissive species in hexane, we have measured spectroscopic properties of perylene dissolved in sulfuric acid. According to previous studies, polycyclic aromatic hydrocarbon (PAH) radical cations are easily formed in a significant amount when dissolved in a powerful oxo-acid, such as sulfuric acid.[17,18,39] A comparison between the radical cation absorption spectrum in sulfuric acid and the multiphoton-excited conductance spectrum of perylene in hexane is shown in Figure 7. The major absorption bands, located at approximately 538 and 733 nm, correspond very well with the peaks found in the matrix-isolated spectrum for the D_5 and the D_3 ($^2B_{2g}$) excitation (730 nm).[38] The bands are slightly broader than those of the matrix-isolated perylene radical cation, which is not unexpected. Note that the resonance enhancement in the conductance spectrum turns on in the spectral region that overlaps with the strong ion absorption peak at 538 nm. The perylene/H_2SO_4 absorption spectrum exhibits negligible absorption in the normal perylene neutral absorption region (350−440 nm), which indicates the absence of neutral perylene molecules in this solution. To measure the emission spectrum

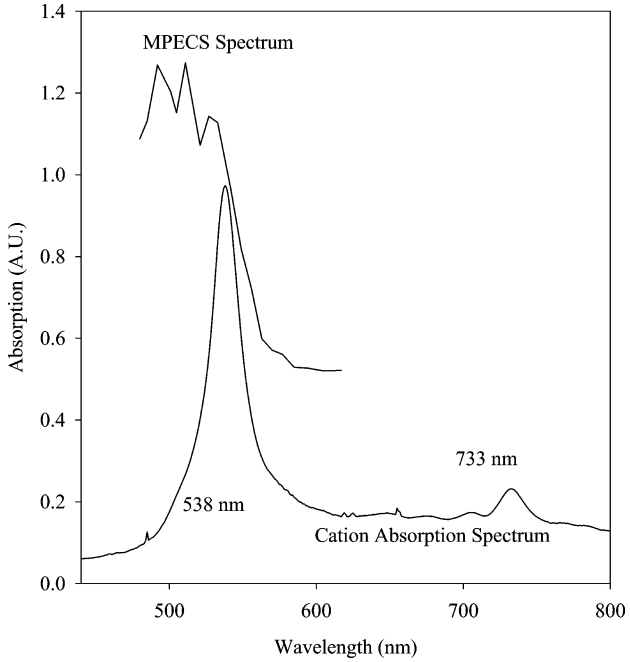

Figure 7. Absorption spectrum of perylene in sulfuric acid. Solution is 5×10^{-5} M perylene. Major absorption bands are at 538 and 733 nm. Included is the multiphoton-excited conductance spectrum (MPECS) of perylene in hexane, which demonstrates the overlap between the (2+1)-REMPI region of perylene and the strong $D_0 \rightarrow D_5$ transition.

of the perylene species present in sulfuric acid under conditions as close as possible to those used in the measurements of perylene in hexane, the femtosecond excitation source was tuned to 535 nm, defocused, and attenuated to decrease the excitation intensity, and thereby discourage multiphoton excitation. The emission spectrum is shown in Figure 6b.

Both spectra exhibit two strong emission peaks at wavelengths greater than 570 nm. The perylene in hexane exhibits peaks at 572 and 596 nm, while the perylene in sulfuric acid exhibits peaks at 585 and 613 nm, resulting in red-shifts of 13 and 17 nm, respectively. A red-shift is expected between the emission peaks in hexane and sulfuric acid. Though the solvatochromic shift is small, it is important to note that in each solvent the emitting and terminal states are both ions, and therefore both states are expected to shift with solvent polarity. This may be the basis of the small, observed solvatochromic shift.

Allamandola observed matrix-isolated perylene radical cation emission in a variety of matrixes at a temperature of a few kelvin.[40] Their study of the emission bands focused exclusively on the $D_1 \rightarrow D_0$ fluorescence peaks, occurring at 792 nm and longer wavelengths, and did not report on emission in the 500−600 nm region. Our instrument is presently incapable of observing emission above 750 nm. Gumy and Vauthey[18] also observed emission in the 550−700 nm region of the spectrum of perylene dissolved in H_2SO_4, and assigned the 618 nm peak to emission from the electronically excited protonated cation PeH^{+*} on the basis of the results of Aalbersberg et al.[41] and the observation of a 590 nm peak in the excitation spectrum of the anomalous emission. The protonated cation is expected to be present in low concentration in sulfuric acid solution. Photochemical preparation of PeH^{+*} following femtosecond excitation of the $Pe^{\bullet+}$ offers an alternative route to the preparation of the putative emissive species in sulfuric acid. The additional peak in our spectrum at ~575 nm appears to depend on the concentration of the sulfuric acid and suggests that two species are responsible for the observed emission. This phenomenon is under further investigation.

The similarity of spectra shown in Figure 6 implies that, if the protonated cation is indeed responsible for the 613 nm emission peak observed in H_2SO_4, then the electronically excited radical cation in hexane abstracts a hydrogen from the solvent, forming the emissive species. Gumy and Vauthey measured an excited-state lifetime of less than 35 ps for the perylene radical cation in each of three different solvent environments, which further suggests that the hydrogen abstraction must involve the solvent. Shkrob et al.[16] have highlighted the importance of hydrogen abstraction in polar solvents when the excited radical cation is more basic than the solvent. However, although hydrogen abstraction is exothermic in nonpolar solvents, hole injection appears to be preferred under nanosecond excitation.[13] The schemes considered by Shkrob and Trifunac suggest that hydrogen abstraction may occur through a multistep mechanism, with the possible involvement of both electron and proton transfer, or aryl radical formation and subsequent hydrogen abstraction and proton capture. It may also be possible that under femtosecond excitation, the radical cation is resonantly excited to a higher energy level through a multiphoton process. The mechanism of hydrogen atom abstraction is currently under investigation.

Conclusions

We have presented evidence for the simultaneous generation and excitation of the perylene radical cation in a nonpolar solution via a two-photon resonance in the singlet manifold. The two-photon resonance enhances the fluorescence, as evidenced by an intensity-squared dependence on the excitation power. The three-photon-excited ion current exhibits a similar excitation profile. The two-photon resonance results in an almost 4-fold increase in the ion signal between 560 and 520 nm excitation. The branching ratio for these processes is currently unclear; however, the emission intensity at 450 nm shows little or no dependence on the applied electric field. Further time-resolved spectroscopic studies will be required to elucidate the excitation and relaxation pathways in more detail.

We have also demonstrated that the overlap between the two-photon resonance in the neutral perylene singlet manifold and a single-photon resonance in the radical cation doublet manifold that corresponds to the $D_0 \rightarrow D_5$ transition can result in the generation of electronically excited perylene radical cations. The similarity of the emission spectrum following femtosecond generation of these highly energetic radical cations and the emission spectrum of perylene in sulfuric acid demonstrates that photochemical transformation following preparation of electronically excited perylene radical cations leads to the anomalous emission observed in the spectral region >550 nm. The fact that the ion emission intensity is on the order of the multiphoton-excited one-photon emission spectrum suggests that a large fraction of the electronically excited radical cations undergo the photochemical reaction and that the photoproduct has a large emission quantum yield. We have tentatively assigned this emission to the protonated perylene cation (PeH^+), leading to the conclusion that the excited radical cation abstracts hydrogen from the solvent. The short lifetime of $Pe^{\bullet+*}$ indicates that the reaction occurs on an ultrafast time scale and is consistent with prior evidence demonstrating the stability of $Pe^{\bullet+}$ and the highly reactive nature of $Pe^{\bullet+*}$. Little is known about the mechanism of formation of PeH^+, but our results indicate that it is either prepared photochemically in its excited electronic state or it is formed in its ground state within the time scale of laser pulse width, and subsequently electronically excited by the laser pulse. These issues will be resolved through further time-resolved and

solvent-dependent spectroscopic studies. Although the phenomena described in this paper appear at first glance to be the result of a rather unique spectral coincidence, we are investigating the applicability of this reaction scheme to a range of PAHs.

Acknowledgment. The laser system used for this investigation was purchased with funds provided in part by the National Science Foundation (CHE-9708896).

References and Notes

(1) Shear, J. B.; Xu, C.; Webb, W. W. *Photochem. Photobiol.* **1997**, *65*, 931.
(2) Gostkowski, M. L.; Curey, T. E.; Okerberg, E.; Kang, T. J.; Bout, D. A. V.; Shear, J. B. *Anal. Chem.* **2000**, *72*, 3821.
(3) Yamada, S.; Ogawa, T. *Anal. Chim. Acta* **1986**, *183*, 251.
(4) Ogawa, T.; Ogawa, T.; Nakashima, K. *J. Phys. Chem. A* **1998**, *102*, 10608.
(5) Ogawa, T.; Sato, M.; Tachibana, M.; Ideta, K.; Inoue, T.; Nakashima, K. *Anal. Chim. Acta* **1995**, *299*, 355.
(6) Ogawa, T.; Chen, H.; Inoue, T.; Nakashima, K. *Chem. Phys. Lett.* **1994**, *229*, 328.
(7) Ogawa, T.; Kise, M.; Yasuda, T.; Kawazumi, H.; Yamada, S. *Anal. Chem.* **1992**, *64*, 1217.
(8) Kawazumi, H.; Isoda, Y.; Ogawa, T. *J. Phys. Chem.* **1994**, *98*, 170.
(9) Nakashima, K.; Kise, M.; Ogawa, T.; Kawazumi, H.; Yamada, S. *Chem. Phys. Lett.* **1994**, *231*, 81.
(10) Brede, O.; Leichtner, T.; Kapoor, S.; Naumov, S.; Hermann, R. *Chem. Phys. Lett.* **2002**, *366*, 377.
(11) Liu, A.; Loffredo, D. M.; Trifunac, A. D. *J. Phys. Chem.* **1993**, *97*, 3791.
(12) Shkrob, I. A.; Sauer, M. C., Jr.; Schmidt, K. H.; Liu, A. D.; Yan, J.; Trifunac, A. D. *J. Phys. Chem. A* **1997**, *101*, 2120.
(13) Shkrob, I. A.; Sauer, M. C., Jr.; Trifunac, A. D. *J. Phys. Chem. B* **1999**, *103*, 4773.
(14) Shkrob, I. A.; Sauer, M. C., Jr.; Trifunac, A. D. *J. Phys. Chem.* **1996**, *100*, 7237.
(15) Shkrob, I. A.; Sauer, M. C., Jr.; Yan, J.; Trifunac, A. D. *J. Phys. Chem.* **1996**, *100*, 6876.
(16) Shkrob, I. A.; Sauer, M. C., Jr.; Liu, A. D.; Crowell, R. A.; Trifunac, A. D. *J. Phys. Chem. A* **1998**, *102*, 4976.
(17) Brodard, P.; Sarbach, A.; Gumy, J.-C.; Bally, T.; Vauthey, E. *J. Phys. Chem. A* **2001**, *105*, 6594.
(18) Gumy, J.-C.; Vauthey, E. *J. Phys. Chem. A* **1997**, *101*, 8575.
(19) Peon, J.; Hess, G. C.; Pecourt, J.-M. L.; Yuzawa, T.; Kohler, B. *J. Phys. Chem. A* **1999**, *103*, 2460.
(20) Yu, J. A.; Nocera, D. G.; Leroi, G. E. *Chem. Phys. Lett.* **1990**, *167*, 85.
(21) Greever, J.; Turner, J. B. M.; Kauffman, J. F. *J. Phys. Chem. A* **2001**, *105*, 8635.
(22) Shear, J. B. *Anal. Chem.* **1999**, *71*, 598A.
(23) Matsunuma, S.; Akamatsu, N.; Kamisuki, T.; Adachi, Y.; Maeda, S.; Hirose, C. *J. Chem. Phys.* **1988**, *88*, 2956.
(24) Meyer, Y. H.; Plaza, P. *Chem. Phys.* **1995**, *200*, 235.
(25) Birks, J. B. *Photophysics of Aromatic Molecules*; John Wiley & Sons: London, 1970.
(26) Siebbeles, L. D. A.; Emmerichs, U.; Hummel, A.; Bakker, H. J. *J. Chem. Phys.* **1997**, *107*, 9339.
(27) Tobita, S.; Leach, S.; Jochims, H. W.; Ruehl, E.; Illenberger, E.; Baumgaertel, H. *Can. J. Phys.* **1994**, *72*, 1060.
(28) Qiu, D.; Shenkin, P. S.; Hollinger, F. P.; Still, W. C. *J. Phys. Chem. A* **1997**, *101*, 3005.
(29) Bondi, A. *J. Phys. Chem.* **1964**, *68*, 441.
(30) Katoh, R.; Lacmann, K.; Schmidt, W. F. *Z. Phys. Chem.* **1995**, *190*, 193.
(31) Siomos, K.; Kourouklis, G.; Christophorou, L. G.; Carter, J. G. *Radiat. Phys. Chem.* **1980**, *15*, 313.
(32) Siomos, K.; Christophorou, L. G. *Chem. Phys. Lett.* **1980**, *72*, 43.
(33) Siomos, K.; Kourouklis, G.; Christophorou, L. G. *Chem. Phys. Lett.* **1981**, *80*, 504.
(34) Siomos, K.; Kourouklis, G.; Christophorou, L. G.; Carter, J. G. *Radiat. Phys. Chem.* **1981**, *17*, 75.
(35) Holroyd, R. A.; Preses, J. M.; Zevos, N. *J. Chem. Phys.* **1983**, *79*, 483.
(36) Inoue, T.; Sasaki, S.-Y.; Tokeshi, M.; Ogawa, T. *Chem. Lett.* **1998**, 609.
(37) Jiang, Y.; Blanchard, G. J. *J. Phys. Chem.* **1994**, *98*, 9417.
(38) Chillier, X. D. F.; Stone, B. M.; Salama, F.; Allamandola, L. J. *J. Chem. Phys.* **1999**, *111*, 449.
(39) Shi, J.-L.; Zhou, C.-M.; Zhao, X.; Xu, J.-Y.; Jiang, X.-K. *Chin. J. Chem.* **2001**, *19*, 154.
(40) Joblin, C.; Salama, F.; Allamandola, L. *J. Chem. Phys.* **1995**, *102*, 9743.
(41) Aalbersberg, W. I.; Hoijtink, G. J.; Mackor, E. L.; Weiland, W. P. *J. Chem. Soc.* **1959**, 3049.